Low-energy electron scattering from methylene radicals: Multichannel-coupling effects

Kedong Wang,* Haoxing Zhang, Xiaotian Huang, Yufang Liu, and Jinfeng Sun
College of Physics and Materials Science, Henan Normal University, Xinxiang 453007, People's Republic of China

(Received 29 September 2017; published 12 January 2018)

We reported elastic (integrated and differential), momentum-transfer, and excitation cross sections for electron collisions with methylene radical. R-matrix method is employed to calculate the cross section for electron energies ranging from 0.01 to 15 eV. The results of 1-state, 3-state, 15-state, 20-state, and 24-state close-coupling (CC) approximations are presented. We detect two shape resonances and three Feshbach resonances in the 24-state CC approximation. We discuss the multichannel-coupling effects on the calculated cross sections and resonances, and how the number of excited states included in the target state impacts the convergence of the elastic and the $X\,^3B_1 \rightarrow 1\,^1A_1$ and $X\,^3B_1 \rightarrow 1\,^1B_1$ excitation cross sections, especially at higher impact energy. Finally, we estimate the accuracy of the $1\,^1A_1$ and $1\,^1B_1$ excitation cross sections.

DOI: 10.1103/PhysRevA.97.012703

I. INTRODUCTION

Electron-molecule collisions are of fundamental importance and have many useful applications for plasma physics, laser physics, atmospheric and interstellar models, isotope separation, radiation physics, and magnetohydrodynamics (MHD) power generation [1,2]. The design of plasma reactors is still based on empirical studies due to lack of reliable cross sections for electron-molecule scattering. The accurate simulation of electron-molecule scattering still remains a great computational challenge. One of the difficulties is how to define a proper balance between the electronic excitation and polarization to describe the scattering $N + 1$ electrons system problem. Separation of the nuclear motion from the scattering dynamics caused by the electronic cloud in a fixed nuclei approximation is the usual strategy to simplify the problem. Even at this level of approximation, in molecular targets, the density of electronically excited states is usually so large that the convergence of multichannel scattering calculations could be seriously hindered in many cases of practical interest. This is particularly true for molecules having its first thresholds opening up at 3–4 eV and becomes even more critical with the energy of the incident electron increasing. At low energies, only the elastic channel is electronically open and the distortion of the electronic cloud is taken into account by allowing virtual excitations (closed channel space) from the ground state. As we increase the impact energy, other electronic states (including the discrete and continuum states) can be excited giving rise to the important questions: (1) how many of these states must be included in a calculation in order to predict an accurate cross section? (2) how do these multichannel effects affect the elastic cross sections? (3) how do they affect the other electronic excitation cross sections? and (4) how sophisticated must the electronic states description be in order to accurately calculate the cross sections? Recently, several theoretical groups [3–7] have addressed one or more of these issues using different methods for describing the electronic excitation of molecules by electron impact, at specific levels of multichannel coupling. They denote that there are many challenges that must be overcome to obtain reliable cross sections.

The goal of the present paper, was to provide an extensive dataset of cross sections for elastic scattering as well as electron-impact excitation of methylene radical. Methylene radical is the direct chemical precursor of the widely observed CH radical as well as other carbon-bearing molecules, which makes it of interest to both chemists and astrophysicists [8,9]. It has a high density of electronic states within relatively small excitation energy. For these reasons it is interesting to investigate the low-energy scattering with methylene radical. The organization of this paper is as follows: In Sec. II, we present some details of our calculations. In Sec. III, our calculated results are presented and discussed. Finally, some conclusive remarks are presented in Sec. IV.

II. COMPUTATIONAL DETAILS

A. Theoretical method

There are three widely used approaches for electron scattering calculations: the *ab initio* R-matrix method [10], the complex Kohn variational method [11], and the Schwinger multichannel method [12]. In this work, the R-matrix method is used to study electron scattering by molecules and the UK polyatomic R-matrix codes [2,13] are employed to calculate the cross sections. The R-matrix method works on the principle of division of configuration space into concentric spherical regions, namely, the inner and outer regions. The inner region is defined as the space inside of a sphere of radius r in which the center of mass of the molecule defines the origin of the coordinates. The radius r is chosen in order to have all electronic density of the target molecule inside the sphere. In the inner region, the system is represented by a complex comprised of N electrons of the molecule plus one continuum electron, ($N + 1$ electrons). As the interactions between the scattering electron and all electrons of the molecule are strong in the inner region, it is important to consider exchange,

*wangkd@htu.cn

polarization, and correlation effects. The wave function inside the sphere is represented in the form of a close-coupling (CC) expansion

$$\Psi_k(x_1,\ldots,x_{N+1}) = \mathcal{A}\sum_{ij}\bar{\Phi}_i(x_1,\ldots,x_N;\hat{\mathbf{r}}_{N+1}\sigma_{N+1})\,r_{N+1}^{-1}\,B_j(r_{N+1})\,a_{ijk} + \sum_i \chi_i(x_1,\ldots,x_{N+1})\,b_{ik}. \quad (1)$$

here $\bar{\Phi}_i$ denotes the channel functions constructed from the N-electron target states, and $\mathcal{A}$ is an antisymmetrization operator, while x_N is the spatial and spin coordinate of the Nth electron, represents the ith state of the N-electron target, and $B_j(r)$ represents the continuum orbitals. The χ_i are additional $(N+1)$-electron bound states. Coefficients a_{ijk} and b_{ik} are variational parameters determined as a result of the matrix diagonalization. The sum in the second term of Eq. (1) represents the short-range correlation and polarization effects, running over all configurations for $(N+1)$ electrons that are L^2 functions. These are also important for relaxing the orthogonality imposed between the target and continuum orbitals.

In the outer region, since the correlation effects are negligible, a long-range multipole expansion is used to represent the electron-target interaction. The R matrix is built at the boundary between the regions, using inner region information, and the one-particle multichannel problem is solved by propagating the R matrix outwards up to a radius large enough so that an asymptotic expansion for the radial wave functions can be matched to known analytical solutions.

In the fixed nuclei (FN) approximation, the elastic cross section of molecules with permanent dipole moment usually diverges in a forward scattering direction. In order to take into account the long-range interaction, a Born closure procedure was employed. In the R-matrix method the continuum orbitals are calculated using partial waves up to $l_{\max}$ and the higher partial waves are included in scattering T matrices via analytical Born T matrices, using the rotating dipole approximation to calculate rotational motion to avoid the divergence of nuclei fixed approximation [14]. For this we used the code POLYDCS [15] which performs a frame transformation from a body-fixed formulation neglecting rotational motion to a space-fixed axis system including the rotational motion and then calculates rotational excitation $(J=0\rightarrow J'=0,1,2,\ldots)$ differential cross sections (DCSs).

B. Target and scattering models

The CH_2 radical is an open-shell system which belongs to the C_{2V} point group. The molecular geometries were optimized at the B3LYP/6-31++G** level. We obtained the $R_{CH}=1.085$ Å and $\angle$(H-C-H) $=135.5^\circ$. They are in good agreement with the experimental results as reported in the Computational Chemistry Comparison and Benchmark Database (CCCBDB) [16]. The Hartree-Fock (HF) self-consistent field (SCF) calculations with cc-pVDZ basis sets for the ground state of methylene were used to obtain the wave function. The electronic configuration at the ground state is $1a_1{}^2 2a_1{}^2 1b_2{}^2 3a_1 1b_1$. The complete active space (CAS) configuration interaction (CI) method was used to represent the target state. In our CI model, two electrons were frozen to the core molecular orbital (MO) $1a_1$. The remaining six electrons are allowed to move freely in 14 MOs ($2a_1$–$8a_1$, $1b_1$–$3b_1$, $1b_2$–$3b_2$, and $1a_2$). The dipole moment of μ value at the ground state is predicted to be 0.210 a.u., which is in agreement with the available theoretical value 0.234 a.u. [17]. The components of the quadrupole moments Q_{20} and Q_{22} are 0.437 and 1.366 a.u., respectively.

TABLE I. The number of configuration state functions (CSFs), vertical excited energies (VEEs) (in eV) for the target states of CH_2, and static dipole moment (μ) for the ground state (in Debye).

State	N	CAS	Theory	Expt.
X^3B_1	15792	0	0	
1^1A_1	10621	1.16	0.43,[1] 0.47,[2] 0.39[3]	0.39[4]
1^1B_1	10304	1.73	1.43,[1] 1.56,[2] 1.44[3]	1.42[4]
2^1A_1	10621	3.49	2.54,[1] 2.72,[2] 2.56[3]	
1^3A_2	15840	7.41	7.28,[1] 7.30,[5] 7.56[6]	
1^3A_1	15639	7.51	6.43,[1] 6.38[6]	
1^3B_2	15792	7.93	7.76,[1] 7.93,[5] 8.15[6]	
3^1A_1	10621	8.14		
1^1A_2	10176	8.48		
2^3B_1	15792	8.68	7.92,[1] 7.82[6]	7.95[7]
1^1B_2	10304	9.03	7.91,[5] 8.78[3]	
2^1B_1	10304	9.36		
2^3B_2	15792	9.93		
2^1B_2	10304	10.38		
2^3A_2	15840	11.00		
$\mu(X^3B_1)$		0.53	0.59[3]	

[1].From Ref. [21].
[2].From Ref. [19].
[3].From Ref. [17].
[4].From Ref. [18].
[5].From Ref. [20].
[6].From Ref. [22].
[7].From Ref. [23].

Table I lists the predominant configurations, the number of configuration state functions (CSFs), and vertical excited energies (VEEs) for the first 15 states. The remaining nine excited states are not shown as these are included to check the convergence of our results and also to avoid any unphysical pseudoresonances that may otherwise appear in the cross section. The first electronic excited energy of CH_2 is 1.16 eV, which is obviously higher than the experimental value of 0.39 eV [18] and the other theoretical adiabatic excitation energies varying from 0.39–0.47 eV [17,19,21]. This large difference comes from the fact that the large structural relaxation occurs when one measures or calculates the adiabatic excitation energies, such as Li *et al.* [21] optimized the structure of the first electronic excited state for CH_2 and obtained the $\angle$(H-C-H) of 102.4°, which shows more bent structure than our ground-state structure [$\angle$(H-C-H) $=135.5^\circ$]. Our calculated VEE of 1.73 eV for the second excited state is in agreement with the experimental value of 1.42 eV [18] and the available calculated values of 1.43–1.56 eV [17,19,21]. For the third excited state, the deviations between our result and other theoretical results are about 1.0 eV, which is also due to the different structure used in the calculation, as shown in Ref. [21].

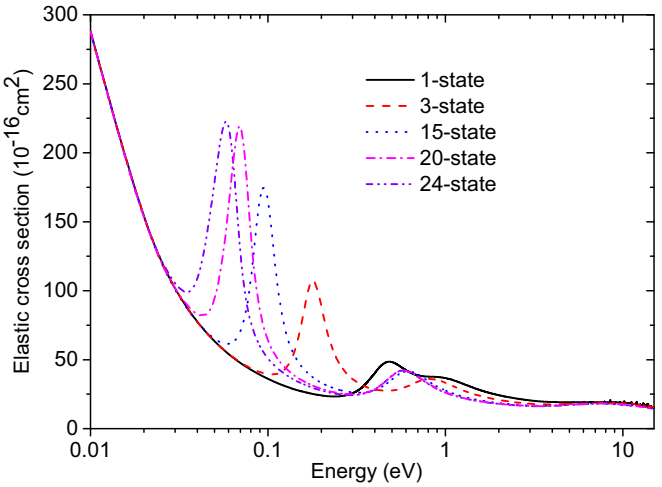

FIG. 1. Elastic cross section for 1-state, 3-state, 15-state, 20-state, and 24-state CC calculations in the energy range of 0.01–15 eV.

For the fourth excited energy, our predicted value of 7.41 eV is in good agreement with the available theoretical values varying from 7.28 to 7.56 eV [19,21,22].

The scattering calculations have been carried out by retaining 12 singlet plus 12 triplet states with the doublet A_1, A_2, B_1, and B_2 symmetries and 12 triplet states with the quartet A_1, A_2, B_1, and B_2 symmetries in the expansion (1). All the target states are represented by CI wave functions and the states with VEE not more than 11.0 eV are given in Table I (two $^3A_1$ and $^1A_2$, one $^1B_1$, $^1B_2$, $^3A_2$, $^3B_1$, and $^3B_2$ are not shown in the table). The continuum orbitals of [24], represented by Gaussian-type orbitals (GTOs) centered at the molecular center of mass, have been used. Our calculations were performed for the continuum orbitals up to g partial waves. These continuum orbitals are orthogonalized to the target orbitals, and the continuum orbitals with an overlap of less than 1.0×10^{-7} were removed [25]. It is very important to balance the correlations included in the target states and those in the scattering calculations. This is achieved by allowing seven electrons (six valance electrons plus one scattering electron) to move freely among 14 MOs ($2a_1$– $8a_1$, $1b_1$–$3b_1$, $1b_2$–$3b_2$, and $1a_2$).

III. RESULTS

A. Elastic scattering cross section

Figure 1 shows elastic cross section for 1-state, 3-state, 15-state, 20-state, and 24-state CC calculations in the energy range of 0.01–15 eV. Two peaks are observed at 0.51 and 1.24 eV in the 1-state CC model. Taking the multichannel coupling into account, the positions of these two peaks go down to 0.18 and 0.88 eV in the 3-state CC model, to 0.09 and 0.65 eV in the 15-state CC model, and to 0.07 and 0.64 eV in the 20-state CC model. Clearly, with increasing the target states in the CC calculation, the positions of these two resonant peaks decrease. The retention of a large number of electronic channels in the CC model provides the necessary polarization potential in an *ab initio* way, which is crucial for determining the resonances and their resonance parameters. With increasing the number of electronic channels, the 24-state CC model

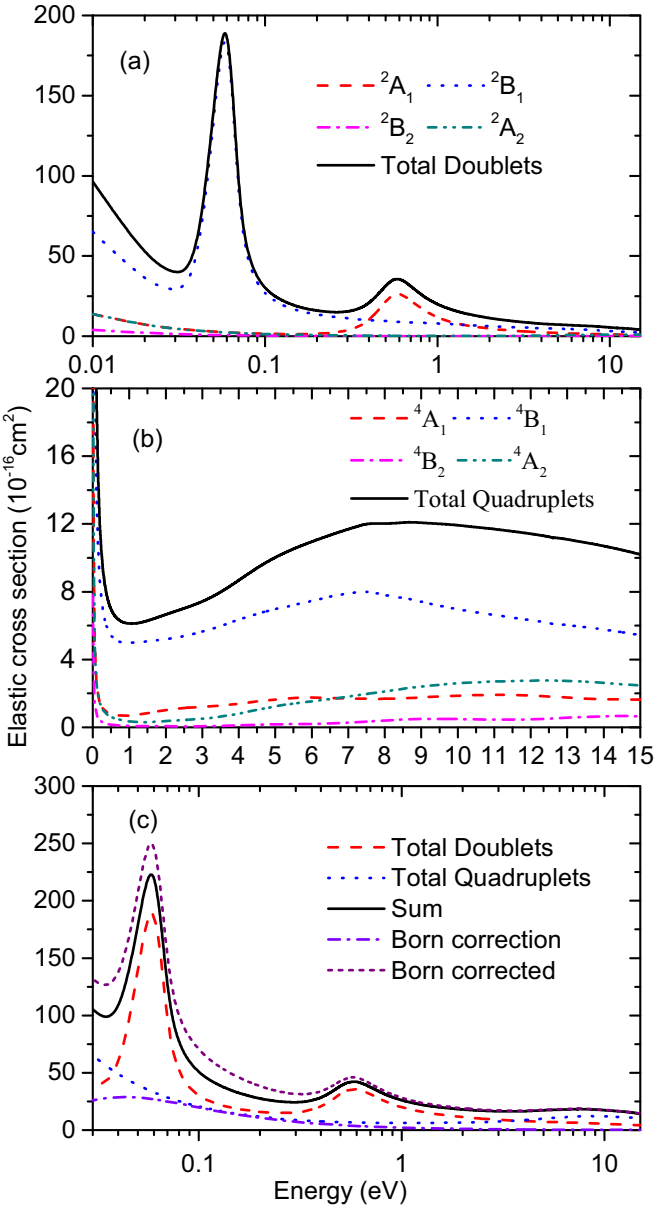

FIG. 2. Elastic cross sections in the energy range of 0.01–15 eV. (a) Doublet A_1, B_1, B_2, and A_2 components and total doublets. (b) Quadruplet A_1, B_1, B_2, and A_2 components and total quadruplets. (c) Total doublets, total quadruplets, total doublet plus total quadruplet (Sum), Born correction, and Born corrected.

gives almost convergent resonant peaks at 0.06 and 0.64 eV. All the CC calculations detect two shape resonances, but the 24-state CC calculations give the most accurate values of their resonance parameters. It should be noted that the very small differences observed between the elastic cross sections of 20-state and 24-state calculations indicate the convergence of coupled-channels results of the present 24-state calculation for the elastic scattering.

Figure 2 shows the four component cross sections (both doublet and quadruplet) for 24-state CC results, together with the summed elastic integral and Born-corrected cross sections. The $^2B_1$ and $^4B_1$ components play the most important role in the elastic cross sections for the doublet and quadruplet

TABLE II. Parameters of identified e-CH_2 resonances (in eV).

State	Classification	Type	Position	Width	Parent state
$^2B_1$	$1b_2{}^2 3a_1{}^2 1b_1$	Shape	0.05	0.03	X^3B_1
$^2A_1$	$1b_2{}^2 3a_1 1b_1{}^2$	Shape	0.64	0.53	X^3B_1
$^2B_2$	$1b_2 3a_1{}^2 1b_1{}^2$	Feshbach	7.35	0.04	1^3A_2
$^2A_1$	$1b_2{}^2 3a_1{}^2 4a_1$	Feshbach	7.48	0.02	1^3A_1
$^2B_1$	$1b_2{}^2 3a_1{}^2 2b_1$	Feshbach	8.63	0.01	2^3B_1

components, respectively. Two peaks are observed around 0.06 and 0.64 eV in the total cross section. We find that the first narrow maximum at 0.06 eV in the $^2B_1$ symmetry belongs to shape resonance with a width of 0.03 eV. The following broad maximum at 0.64 eV in the $^2A_1$ symmetry is also shape resonance with a width of 0.53 eV. As shown in Fig. 2(c), the contribution of Born correction is small, except at very low incident energies. This results from the fact that CH_2 has a small static dipole moment and that the Born correction for the rotational $(0 \rightarrow 1)$ component is significant only at very low energies.

The resonance is defined as the temporary trapping of an electron to form a quasibound short-lived state. It is key for many electron-molecule scattering processes especially at low energies. In the vicinity of a resonance, the cross section often changes sharply with energy, and the eigenphase sum changes by a factor of about π radians in the relatively narrow energy range. By analyzing the eigenphase sums calculated within the 24-state CC model, the resonance parameters (position and width) are obtained and listed in Table II along with their tentative assignments. The parent states and the configurations of resonances are determined by performing a set of calculations including some carefully chosen configurations and by manipulating the active space of calculations. It is known that the energies of resonances are directly linked to the energies of their parent states. As shown in Table I, the differences of VEEs between our present results and the theoretical and experimental results for three triplet states $1\,^3A_2$, $1\,^3A_1$, and 2^3B_1 are about 0.15, 1.13, and 0.73 eV, respectively. These differences for the three parent states will bring the same size deviations for the position of corresponding resonances.

B. Inelastic scattering cross section

Figure 3 presents the electron impact excitation cross sections from the ground state $X\,^3B_1$ to the first three excited states 1^1A_1, 1^1B_1, and 2^1A_1 with the 24-state CC model. According to the optical dipole selection rules, all three of these transitions are spin-forbidden.

The total excitation cross sections of $X\,^3B_1 \rightarrow 1^1A_1$ together with four C_{2V} symmetry components are shown in Fig. 3(a). The large broad peak near threshold around 2.1 eV in the total cross section results from the $^1A_1$ threshold effect. With the increasing energy, two small sharp peaks around 7.35 and 7.48 eV are signatures of the Feshbach resonances with $^2B_2$ and $^2A_1$ symmetries, and their parent states are 1^3A_2 and 1^3A_1 states, respectively. The dip at 8.63 eV in $^2B_1$ symmetry has a width of 0.01 eV and is a Feshbach resonance whose parent state is the 2^3B_1 state of CH_2. The component $^2B_1$ gives the major contributions to the cross sections for this

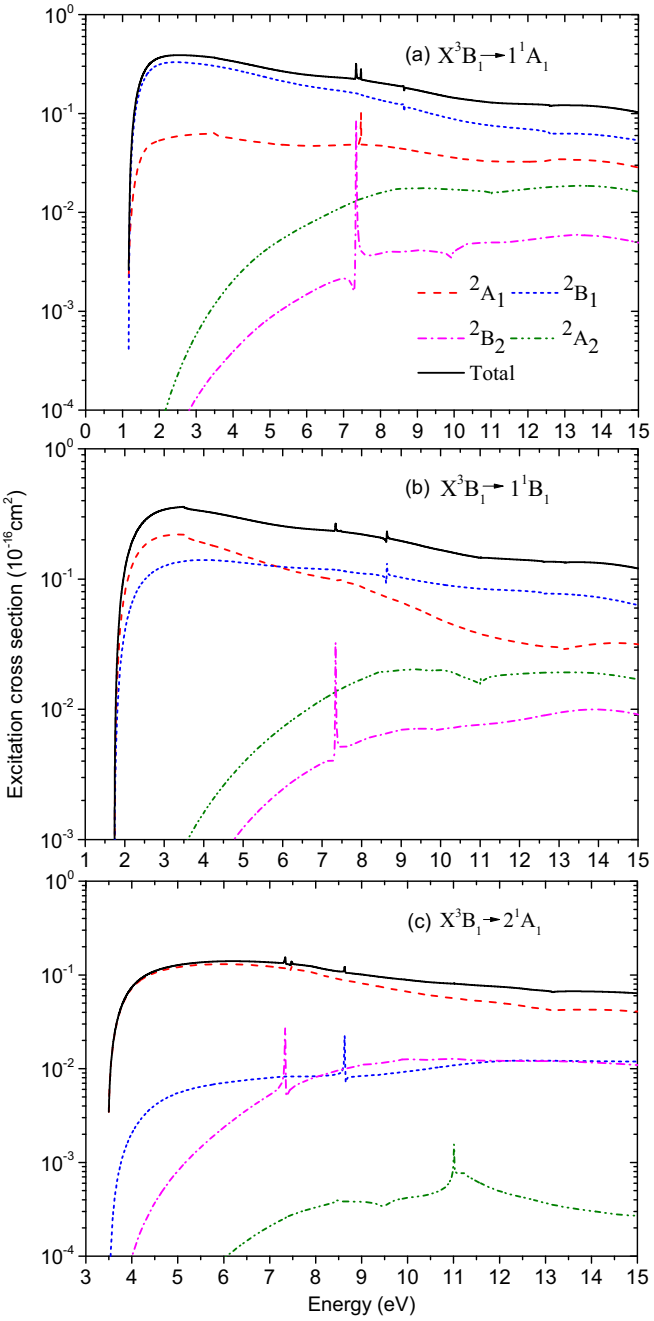

FIG. 3. (a) $X^3B^1 \rightarrow 1^1A_1$ excitation cross sections, (b) $X^3B^1 \rightarrow 1^1B_1$ excitation cross sections, and (c) $X^3B^1 \rightarrow 2^1A_1$ excitation cross sections.

transition. The doublet components and the total excitation cross sections for the excited states 1^1B_1 and $2\,^1A_1$ are shown in Figs. 3(b) and 3(c), respectively. These two excitation cross sections have a similar character to the 1^1A_1 excitation cross section.

Figure 4 presents excitation cross sections from the ground state to the first two excited states for five different models. 3-state, 15-state, 20-state, and 24-state CC models use the CAS: $2a_1$–$8a_1$, $1b_1$–$3b_1$, $1b_2$–$3b_2$, and $1a_2$ (noted by CAS1), while the other 15-state CC model uses a smaller CAS: $2a_1$– $7a_1$, $1b_1$–$2b_1$, $1b_2$–$2b_2$, and $1a_2$ (noted by CAS2). It is

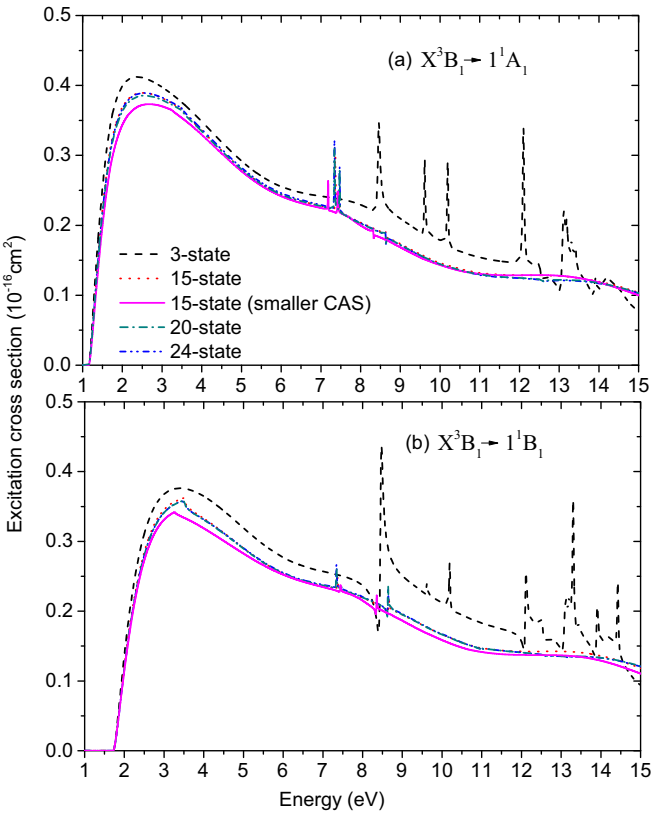

FIG. 4. The excitation cross sections in five different models: 3-state, 15-state, 15-state (with a smaller CAS), 20-state, and 24-state CC calculations. (a) $X^3B^1 \rightarrow 1^1A_1$ excitation cross sections. The 15-state excitation threshold has been shifted lower by 0.28 eV. (b) $X^3B^1 \rightarrow 1^1B_1$ excitation cross sections. The 15-state excitation threshold has been shifted lower by 0.25 eV.

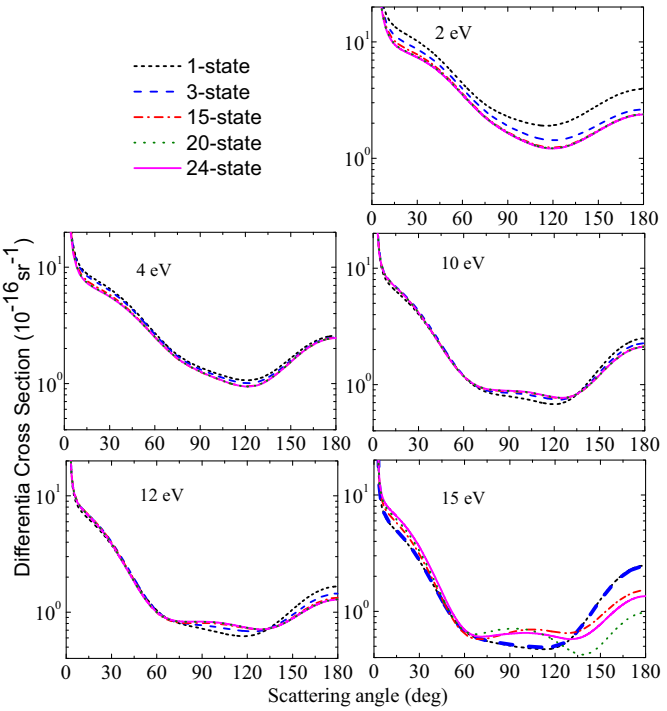

FIG. 5. Difference cross sections of doublet symmetry for elastic scattering at incident energies of 2, 4, 10, 12, and 15 eV with five different models: 1-state, 3-state, 15-state, 20-state, and 24-state CC calculations.

noted that CAS1 produced the excitation thresholds for 1^1A_1 and 1^1B_1 states are lower by 0.28 and 0.25 eV, respectively, than that of CAS2 results, which are closer to the experimental value [18]. With the purpose of investigating the effect of CAS on the cross-section magnitude, the threshold of the 15-state CC calculations in CAS2 is shifted down by 0.28 eV for 1^1A_1 state and 0.25 for the 1^1B_1 state to coincide with that of CAS1. As shown in the picture 4, the very small difference (less than 1%) between the 15-state and 24-state cross sections indicates that the convergence of the excitation cross section results with respect to the size of coupling channels has been reached in the considered energy range for the first two excited states. The large differences between the cross sections of the 3-state and the other models are found and reveal that multichannel-coupling effects on the excited channel is very important for the excited state. For the cross section of the 1^1A_1 excited state as shown in Fig. 4(a), the difference between the cross sections of the 15-state in CAS1 and CAS2 is small (within 1%) in the high-energy region above 3.5 eV, but noticeable (within 6%) in the low-energy region below 3.5 eV. The present CAS1 threshold is higher by about 0.77 eV than the more accurate experimental results [18]. This threshold energy difference may bring an uncertainty of about 17% in our $X^3B^1 \rightarrow 1^1A_1$ excitation cross sections. For the 1^1B_1 excitation cross section shown in Fig. 4(b), the difference between the cross sections of the 15-state in CAS1 and CAS2 is within 10%. Comparing with the experimental result [18], our CAS1 threshold energy difference (0.31 eV) may bring an uncertainty of about 13% in our $X^3B^1 \rightarrow 1^1B_1$ excitation cross sections. It is well known that a larger active space would give rise to additional correlation effects and increase correlation energy, and hence produce accurate excitation thresholds. But it could make the dynamical R-matrix calculations intractable.

C. Differential cross section

The evaluation of DCSs is a stringent test for any scattering theory employed. In the present paper, the K-matrix based on five different CC models is used to calculate the doublet DCSs and to investigate the influence of multichannel effects. All these models produce the same dipole moment (0.53 D) and rotational constants (57.88, 8.29, and 7.25 cm^{-1}) for the target state, which are used to calculate the doublet DCSs.

Figure 5 shows the present calculated doublet DCS at the incident energies of 2, 4, 10, 12, and 15 eV, which is obtained by summing up all the rotationally elastic and inelastic DCSs with J up to 5 for each incident energy. As shown in the figure, for the energies of 2 eV the presence of multichannel effects substantially changes the DCS when compared to the one obtained at the 1-state CC model. At the incident energies of 2, 4, 10, and 12 eV, the great similarity of the curves corresponding to the 15-state, the 20-state, and the 24-state CC models provides an indication that a good convergence with respect to multichannel coupling has been achieved to the elastic channel. However, the differences among the DCSs of the 15-state, the 20-state, and the 24-state CC models are

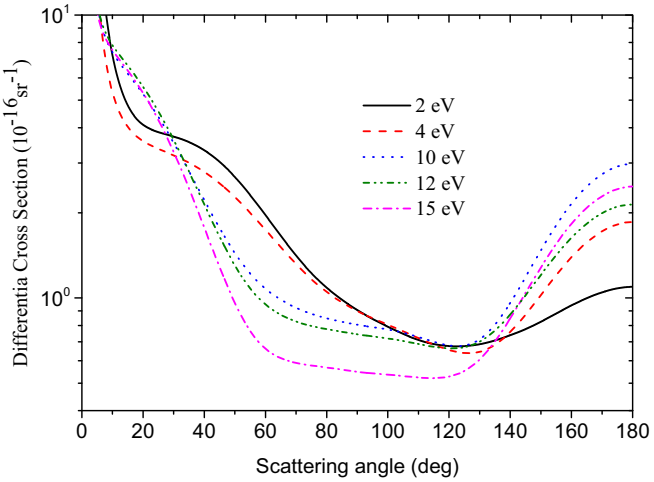

FIG. 6. Total difference cross sections for elastic scattering at incident energies of 2, 4, 10, 12, and 15 eV for the 24-state CC model.

evident at 15 eV, especially in the large scattering angle region (120°–180°), which demonstrates that it is necessary for more target states to be included in the CC calculations to obtain the convergent elastic DCS for higher energy electron impact. da Costa *et al.* studied the multichannel-coupling effects on the cross section for ethylene [5] and phenol [6], and denoted that the better agreement with the experimental cross sections was obtained with increasing the number of channels, especially at the higher energies. Unfortunately, we cannot take more channels into account in the CC calculation here because the 24-state is the largest number of target states which can be used within the present CAS1.

The total spin-averaged DCS for elastic electron scattering from the CH_2 radical is also calculated by using the statistical weight 2/6 for doublet and 4/6 for quartet scattering channels. We then use the following formula to calculate the DCS:

$$\frac{d\sigma}{d\omega} = \frac{1}{3}\left[2\left(\frac{d\sigma}{d\omega}\right)^{Q} + \left(\frac{d\sigma}{d\omega}\right)^{D}\right], \tag{2}$$

where $(\frac{d\sigma}{d\omega})^{Q,D}$ represents the DCS for the quartet and doublet cases, respectively.

Figure 6 shows the present calculated spin-averaged DCS at the incident energies of 2, 4, 10, 12, and 15 eV with the 24-state CC model. The large cross sections in the forward direction are due to the dipolar nature of the target. The state-resolved cross sections (discussed below) show that the pure elastic ($0 \rightarrow 0$) transition is responsible for the appearance of the minimum in the summed cross section in the medium scattering angle region (100°–140°), which indicates the crucial role of the short-range interactions in the backward scattering region. To the best of our knowledge, there is no experimental or theoretical DCS data for this molecule available for comparison.

The state-resolved doublet and quartet cross sections at 2.0 eV are shown in Fig. 7. The elastic and inelastic ($J = 0 \rightarrow J' = 2$) contributions are the main contributions to the total DCS. The cross-section contributions of $J' = 5$ are negligible, thus showing that our DCS has almost converged with respect to the J' value. The momentum-transfer cross section (MTCS) Q_m can be calculated through the data of DCS ($q_{\rm elas}$) and be

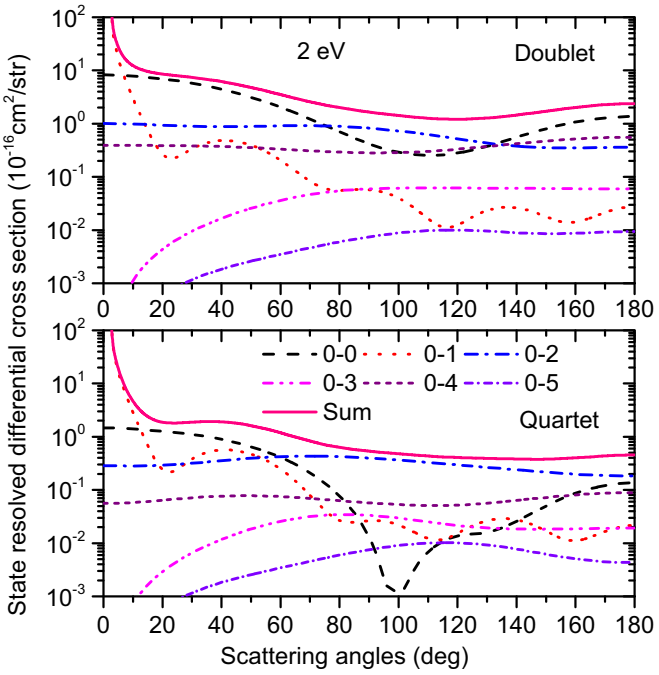

FIG. 7. State-resolved differential cross sections at 2.0 eV.

given by

$$Q_m = 2\pi \int_0^{\pi} (1 - \cos\theta) q_{\rm elas}(\theta) \sin\theta \, d\theta. \tag{3}$$

The MTCS indicates the weights of backward scattering and is useful in the study of electrons drifting through a molecular gas. In contrast to the diverging nature of the DCS in the forward direction (at the small scattering angles), MTCS shows no singularity due to the multiplicative factor $(1 - \cos\theta)$, where θ is the scattering angle. Figure 8 presents our calculated MTCS at five levels of CC approximations (1-state, 3-state, 15-state, 20-state, and 24-state) for the CH_2 radical. Two shape resonances are responsible for the corresponding peaks observed in the MTCS in the energy region below 1.2 eV.

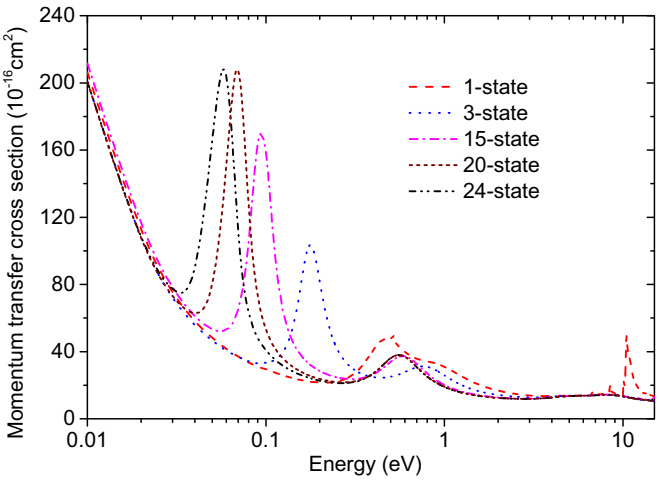

FIG. 8. Momentum transfer cross section in the energy range of 0.01–15 eV.

The change in position of the resonance peaks is attributed to a variation in multichannel-coupling effects in different CC models. About the same trend is also seen in Fig. 1 for elastic integral cross sections.

IV. SUMMARY

We report the elastic integral, differential, momentum transfer, and excitation cross sections of the low-energy electron collision with methylene radical using the R-matrix method at CC approximations. The calculations have revealed the presence of two shape and three Feshbach resonances. Through analyzing the results of 1-state, 3-state, 15-state, 20-state, and up to 24-state CC approximations, the influence of multichannel-coupling effects on the cross-section results is studied. We find multichannel coupling has a substantial effect on the resonance parameters and more target states are needed to include in the CC calculations in order to obtain the convergent cross section. This effect becomes even more important at higher impact energy.

The threshold energy difference of 0.77 and 0.31 eV between our calculations and those of Ref. [18] may introduce a 17% uncertainty in the $X^3B^1 \rightarrow 1^1A_1$ excitation cross section and a 13% uncertainty for the $X^3B^1 \rightarrow 1^1B_1$ excitation cross section. As far as we know, there are no experimental or theoretical cross sections available for comparison. We hope the present work motivates further investigations on electron collisions with the molecule.

ACKNOWLEDGMENTS

This work is supported by the Foundation of National Natural Science Foundation of China (Grants No. U1504109 and No. 11604085) and Science Foundation for the Excellent Youth Scholars of Henan Normal University (Grant No. YQ201601).

[1] R. K. Janev and H. W. Drawin, *Atomic and Plasma-Material Interaction Processes in Controlled Thermonuclear Fusion* (Elsevier, Amsterdam, 1993).
[2] J. Tennyson, Phys. Rep. **491**, 29 (2010).
[3] Z. Masín, J. D. Gorfinkiel, D. B. Jones, S. M. Bellm, and M. J. Brunger, J. Chem. Phys. **136**, 144310 (2012).
[4] T. N. Rescigno and A. E. Orel, Phys. Rev. A **88**, 012703 (2013).
[5] R. F. da Costa, M. H. F. Bettega, M. T. do N. Varella, E. M. de Oliveira, and M. A. P. Lima, Phys. Rev. A **90**, 052707 (2014).
[6] R. F. da Costa, E. M. de Oliveira, M. H. F. Bettega, M. T. do N. Varella, D. B. Jones, M. J. Brunger, F. Blanco, R. Colmenares, P. Limão-Vieira, G. García, and M. A. P. Lima, J. Chem. Phys. **142**, 104304 (2015).
[7] K. Wang, S. Guo, J. Meng, X. Huang, and Y. Wang, Phys. Rev. A **94**, 032703 (2016).
[8] J. M. Hollis, P. R. Jewell, and F. J. Lovas, Astrophys. J. **438**, 259 (1995).
[9] T. J. Millar, P. R. A. Farguhar, and K. Willacy, Astron. Astrophys. Suppl. Ser. **121**, 139 (1997).
[10] P. G. Burke and K. A. Berrington, *Atomic and Molecular Processes: An R-matrix Approach* (Institute of Physics, Bristol, 1993).
[11] T. N. Rescigno, B. H. Lengsfield, C. W. McCurdy, and S. D. Parker, Phys. Rev. A. **45**, 7800 (1992).
[12] K. Takatsuka and V. McKoy, Phys. Rev. A. **30**, 1734 (1984).
[13] J. M. Carr, P. G. Galiatsatos, J. D. Gorfinkiel, A. G. Harvey, M. A. Lysaght, D. Madden, Z. Masin, M. Plummer, J. Tennyson, and H. N. Varambhia, Eur. Phys. J. D **66**, 58 (2012).
[14] F. A. Gianturco and A. Jain, Phys. Rep. **143**, 347 (1986).
[15] N. Sana and F. A. Gianturco, Comput. Phys. Commun. **114**, 142 (1998).
[16] Computational Chemistry Comparison and Benchmark Database, `http://cccbdb.nist.gov`.
[17] Y. Yamaguchi, C. D. Sherrill, and H. F. Schaefer, III, J. Phys. Chem. **100**, 7911 (1996).
[18] P. Jensen and P. R. Bunker, J. Chem. Phys. **89**, 1327 (1988).
[19] Y. Yamaguchi and H. F. Schaefer, III, Chem. Phys. **225**, 23 (1997).
[20] Y. Yamaguchi, H. F. Schaefer, III, J. Chem. Phys. **106**, 1819 (1997).
[21] B.-T. Li, Z.-Z. Wei, and H.-S. Wu, J. Comput. Chem. **33**, 2498 (2012).
[22] J. Römelt, S. D. Peyerimhoff, and R. J. Buenker, Chem. Phys. **54**, 147 (1981).
[23] K. K. Irikura, R. D. Johnson, and J. W. Hudgens, J. Phys. Chem. **96**, 6131 (1992).
[24] A. Faure, J. D. Gorfinkiel, L. A. Morgan, and J. Tennyson, Comput. Phys. Commun. **144**, 224 (2002).
[25] L. A. Morgan, C. J. Gillan, J. Tennyson, and X. Chen, J. Phys. B **30**, 4087 (1997).